Hybrid PET-MR list-mode kernelized expectation maximization reconstruction for quantitative PET images of the carotid arteries

Daniel Deidda, *Student Member, IEEE*, Nicolas Karakatsanis, *Senior Member, IEEE*, Philip M. Robson, Nikos Efthimiou, *Member, IEEE*, Zahi A. Fayad, Robert G. Aykroyd, Charalampos Tsoumpas, *Senior Member, IEEE*

Abstract—Ordered subsets expectation maximization (OSEM) has been widely used in PET imaging. Although Bayesian algorithms have been shown to perform better, they are still not used in the clinical practice due to the difficulty of choosing appropriate and robust regularization parameters. The recently introduced kernelized expectation maximization (KEM) has shown some promise to work successfully for different applications. Therefore, we propose a list mode hybrid KEM (LM-HKEM) for static reconstructions, which we implemented in the open source Software for Tomographic Image Reconstruction (STIR) library. The proposed algorithm uses both MR and PET update images to create a feature vector for each voxel in the image, which contains the information about the local neighborhood. So as not to over-smooth the reconstructed images a 3×3×3 voxels kernel was used. Three real datasets were acquired with the Siemens mMR: a phantom to validate the algorithm and two patient carotid artery studies to show the possible applications of the method. The reconstructed images are assessed and compared for different algorithms: OSEM, OSEM with median root prior (MRP), KEM and LM-HKEM. The results show better quantification performance for the phantom low count images with around 4% bias compared to 7% for KEM and over 11% for OSEM and OSEM with (MRP). Our results show that the proposed technique can be used to improve quantification at low-count condition and it shows promising performance in terms of stability as for different subsets, with comparable number of events, we used the same parameters values. Emphasis is given on the reconstruction of the carotid artery and the characterization of atherosclerosis.

I. INTRODUCTION

Tomographic image reconstruction in PET, nowadays is mostly performed using iterative techniques. Some of them use prior information to model the noise. One way to introduce prior information into the PET reconstruction problem is the Bayesian method [1, 2, 3, 4, 5]. In clinical

practice, however, mostly no prior information is used as regularization can be time demanding and it is preferred to use ordered subsets expectation maximization (OSEM) [13, 14, 15, 16, 17] with Gaussian post-filtering. Recent studies have introduced a different approach called the kernel method [18, 19, 20, 21, 22, 23, 24] which has been shown to give better performance than Bayesian methods. For this reason, this work aims to propose a Kernel Method, which makes use of anatomical information, able to improve image reconstruction in the clinical environment while avoiding the aforementioned problems related to regularization. In this work emphasis is given on quantification for low-count condition, which has shown to be challenging due to bias, noise and contrast losses [5, 25, 26, 27, 28].

Our method is suitable for static reconstruction at different count levels. The LM reconstruction is particularly convenient for low-count images as it helps to speed up the reconstruction. The kernel matrix consists of two terms, which are derived from PET and MR. The PET part is taken from the iterative update using a similar approach as Maximum a Posteriori (MAP). As a result, this part of the kernel depends on the iteration number. Such a procedure avoids the need for a preliminary reconstruction from high count PET data, as in other work, without affecting the convergence rate. In addition, the hybrid nature of the algorithm makes it possible to model the noise in the projection domain while maintaining good resolution. The algorithm has the same form as OSEM with the image being written as a linear combination of a kernel matrix $\boldsymbol{K}$ and a coefficient vector, $\boldsymbol{\alpha}$, $\boldsymbol{\lambda} = \boldsymbol{K}\boldsymbol{\alpha}$. Estimation of $\boldsymbol{\alpha}$ then uses the update equation

$$\alpha_f^{(n+1)} = \frac{\alpha_f^{(n)}}{\sum_j k_{fj} \sum_i p_{ij}} \sum_j k_{fj} \sum_i p_{ij} \frac{1}{\sum_l p_{il} \sum_f k_{fl}\alpha_f^{(n)} + a_i} \quad (1)$$

where α_f is the estimated f^{th} voxel value and p_{ij} is the ij^{th} element of the system matrix. This represents the probability that an event occurring in voxel j produces a coincidence in the ith pair of detectors, a_i is the additive sinogram containing scatter and random events, and k_{fj} is the fj^{th} element of the kernel matrix.

$$k_{fj} = k_m(\boldsymbol{v}_f, \boldsymbol{v}_j) \cdot k_p^n(\boldsymbol{z}_f^n, \boldsymbol{z}_j^n) \quad (2)$$

where

$$k_m(\boldsymbol{v}_f, \boldsymbol{v}_j) = \exp\left(-\frac{\|\boldsymbol{v}_f - \boldsymbol{v}_j\|^2}{2\sigma_m^2}\right) \exp\left(-\frac{\|\boldsymbol{x}_f - \boldsymbol{x}_j\|^2}{2\sigma_{dm}^2}\right) \quad (3)$$
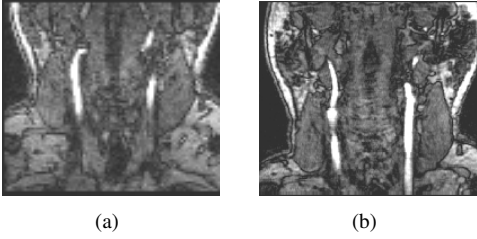
Fig. 1. Slices of the MR images used to estimate the kernel matrix for (a) FDG and (b) NaF studies.

is the kernel coming from the MR image and

$$k_p^n(z_f^n, z_j^n) = \exp\left(-\frac{\|z_f^n - z_j^n\|^2}{2\sigma_p^2}\right) \exp\left(-\frac{\|z_f^n - z_j^n\|^2}{2\sigma_{dp}^2}\right) \quad (4)$$

is the part coming from the iterative update. Here the Gaussian kernels function have been modulated by the distance between voxels in the image space. x_j is the position of the jth voxel, and σ_m, σ_p, σ_{dm} and σ_{dp} are scaling parameters for the distances in (3) and (4), and v and z_j^n are the feature vectors extracted from the MR and the PET images respectively. Note that the PET information come from the iterative estimate of the coefficient α^n, thus the feature vector extracted from that depends on the iteration n. For each voxel of the PET image the corresponding feature vectors, $v_j^{(n)}$ and v_j, are extracted from the local neighborhood of the voxel from the MR image and the PET update image respectively. To keep computation time short, we construct a sparse kernel matrix. A cubic neighborood, ν_j, with $N \times N \times N$ voxels was used and the $k_{fj}^{(n)}$ element of the kernel was defined by

$$k_{fj}^{(n)} = \begin{cases} k_m(v_f, v_j) \cdot k_p(z_f^{(n)}, z_j^{(n)}), & v_f, z_f^{(n)} \in \nu_j \\ 0, & \text{otherwise.} \end{cases} \quad (5)$$

Following previous studies, to make it easier to choose the kernel parameters (such as σ_m and σ_p), the feature vector, v_j, is normalized as

$$\bar{v}_j = \frac{v_j}{\text{SD}} \quad (6)$$

for $k_m(v_j, v_l)$, where SD is the standard deviation of the mean voxel value over the whole MR image, and

$$\bar{z}_j^{(n)} = \frac{z_j^{(n)}}{z_{c_j}^{(n)}} \quad (7)$$

for $k_p(z_f^{(n)}, z_j^{(n)})$ where $z_{c_k}^{(n)}$ is the value of the voxel corresponding to the center of the neighborhood of $\lambda_j^{(n)}$. This choice is related to the fact that the first PET image used for the kernel is uniform and the standard deviation is then zero. Moreover the SD grows significantly iteration by iteration. The contribution of the PET image is crucial to take into account regions associated with molecular processes that are not detected with MR, such as atherosclerotic lesions. In this method, in contrast to [21], each feature vector has 1 non zero element. In this way, the calculation of the norm in (3) and (4) simply become the squared difference between neighbouring

voxels. This was chosen to avoid the computation of the norm for every sub-iteration of the algorithm.

II. METHODS AND MATERIAL

A. Phantom and Clinical Data

The data used in this study were acquired with a Siemens Biograph mMR scanner [9] at Mount Sinai Hospital, NY, USA. A NEMA 3D Phantom was used, which was filled with 155 MBq of FDG and acquired over 1 hour. This data was used to validate the proposed algorithm and to find a stable configuration. For this purpose, also a co-registered MR VIBE sequence was acquired which was used for the kernel matrix calculation. The clinical data comes from two patients with atherosclerotic plaques in the carotid arteries. They were injected with FDG, 184 MBq and 189 MBq of NaF respectively, both scanned for 90 minutes. The List Mode (LM) file for each of the datasets was then partitioned so as to obtain a short frame dataset (5 s for the phantom and 30 s for the patients). For the patient the MR part of the kernel is obtained from the images of a TOF MR Angiography sequence, Figures 1(a) and 1(b).

B. Reconstruction Setup

All the datasets were reconstructed with 10 iterations and 21 subsets using LM-HKEM. The parameters discussed in Section I, ν, σ_m, σ_p, σ_{md} and σ_{pd} were chosen from a preliminary study. The values used in this work are reported in Table I. The size of the neighborhood, ν, was chosen to be, $3 \times 3 \times 3$ voxels. The voxel size, $2.087 \times 2.087 \times 2.031$ mm^3, was chosen based on the scanner characteristics.

TABLE I
kernel parameters values
$\sigma_m = 1 \ \sigma_p = 1 \ \nu = 3^3$

	σ_{dm}	σ_{dp}
Phantom 5 s	0.6	0.6
Patients 30 s	0.6	0.6

For comparison the same datasets have been reconstructed also with OSEM as this is the standard used in clinical routine, ordered subsets maximum a posteriori one step late with median root prior (OSMAPOSL-MRP), for simplicity we refer to it as OSEM-MRP, and the kernelised OSEM using only the MR part. Scatter correction was performed as developed by Tsoumpas et al [29] and discussed in more detail by Polycarpou et al [30]. Randoms were estimated from singles, which were calculated from delayed events [31]. The procedures for these evaluations, including attenuation and normalisation corrections [32], make use of Software for Tomographic Image Reconstruction (STIR) library [33] version 3.0. All datasets were reconstructed using span 11.

C. Images Analysis

The comparison was carried out in terms of bias and contrast recovery coefficient (CRC), these figures of merit were assessed for the low-count case. The long acquisition

reconstructed image with 5 iterations was used as the "true" image for the bias and "true" contrast for CRC. Region of interest (ROI) analysis was performed using: a plaque in the left carotid bifurcation segmented from the PET image, and the surrounding tissue ROI is a $14 \times 14 \times 22$ mm^3 parallelogram around the lesion[1] to study the contrast. Finally, for the phantom, two regions were chosen that are reported in Figure 2, together with the other ROIs. Quantitative comparison between algorithms is performed using the following figure of merit definitions for a single ROI:
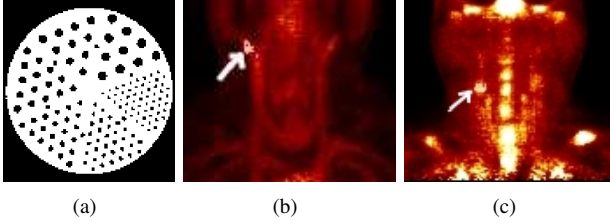

(a)   (b)   (c)

Fig. 2. Regions of interest (ROI) chosen for this study: (a) the phantom target ROI described by the white part, and the background described by the black holes; (b) plaque for patient FDG study and (c) plaque for patient NaF study. The target ROIs are indicated by the white arrows for (b) and (c).

$$\text{bias} = \frac{m - M_T}{M_T} \qquad (8)$$

and

$$\text{CRC} = \frac{m^t - m^b}{C_T} \qquad (9)$$

where m is the mean value over target (hot region) ROIs, m^t is the mean value of the target ROI, m^b is the mean value of the background ROI and C_T is the true contrast estimated from the long acquisition dataset. Note that the bias is only calculated on the phantom ROI.

III. RESULTS

The convergence of the mean activity was studied as a function of the number of iterations in order to see whether the iteration dependent part of the kernel could affect the convergence rate. Figures 3 and 4 show the convergence rate for ten iterations. The values of the kernel parameters are reported in the table I. Figures 3 and 4 also shows the ROI comparison, for the NEMA phantom, between OSEM, OSEM-MRP, KEM using MR and the proposed HKEM in terms of CRC and bias for one 5 s frame. Although the focus of the study is quantification, reconstructed images are also shown. In Figures 5, reconstructed images with OSEM, OSEM plus Gaussian post filter with a 5 mm kernel, OSEM-MRP and the kernelized method with, KEM and HKEM with different values for the kernel parameters σ_{dm} and σ_{dp} are shown for the phantom data. The CRC was also estimated in one atherosclerotic plaque for both FDG and NaF patient studies. Figures 6 and 8 show the CRC in a ROI of the 30 s image for the patient studies using FDG and NaF separately. Image

[1]The part corresponding to the lesion is set to zero by calculating the difference image between the parallelogram and the lesion ROI.
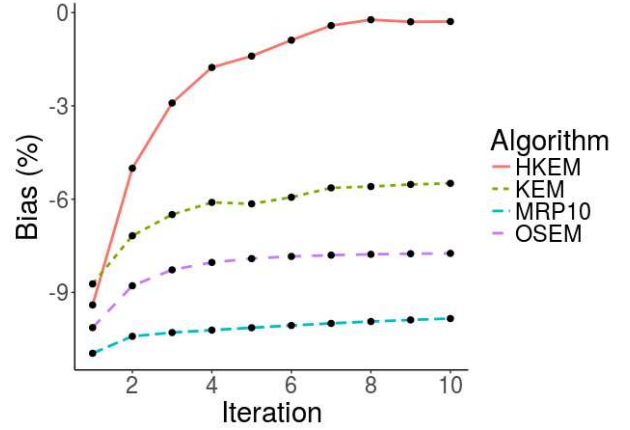

Fig. 3. Quantitative comparison between reconstructed image with EM, EM-MRP, KEM using only MR and the proposed method HKEM for phantom data: bias on a 5 s acquisition.
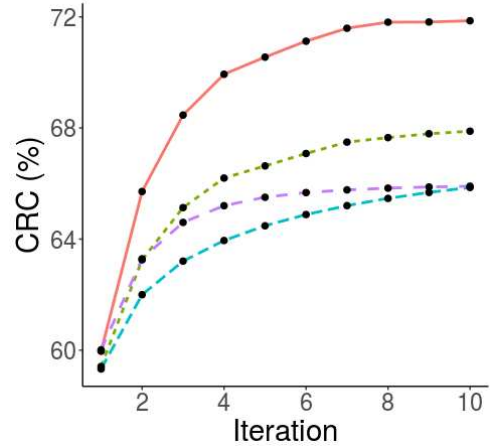

Fig. 4. Quantitative comparison between reconstructed image with EM, EM-MRP, KEM using only MR and the proposed method HKEM for phantom data: CRC on a 5 s acquisition.

quality is also shown in Figure 7 for the FDG study to give an idea of the improvement we obtain with the kernel method and with different parameter values.

IV. DISCUSSION

This work aimed at improving quantification by exploiting the information from both MR and PET images obtained with an hybrid PET-MR scanner. Emphasis was given on those applications that are affected by low count, such as short frames, but potentially also low injected activities. The phantom study showed promising outcomes with respect to bias, as with the proposed method is possible to obtain bias lower than 5%. The LM-HKEM method outperforms the others in terms of bias and CRC, however when it comes to low count it is noisier than the KEM as the kernel contains also the noise. These results are consistent with all the datasets we used, phantom, patient FDG, and patient NaF (Figures 3, 4, 6 8). The results for the convergence study show that if we choose the parameters carefully the rate is not affected.
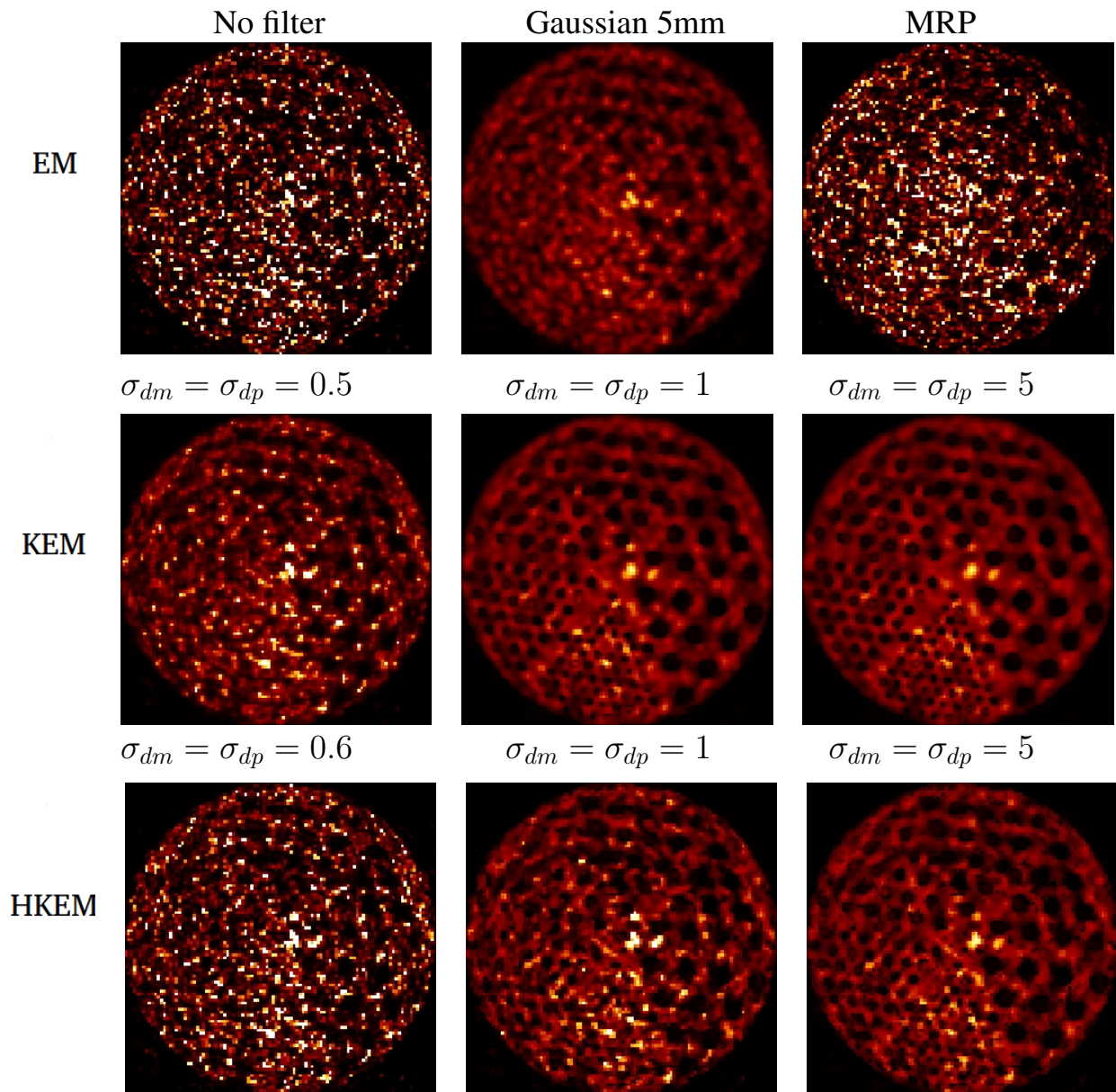
Fig. 5. Reconstructed images with OSEM, OSEM-MRP, KEM using only MR and the proposed method LM-HKEM for 5s frame of the phantom data.

Figures 3 and 4 show that convergence rate is higher for the kernel method during the early iterations but it reaches similar values as OSEM after the 6th iteration. In addition, we noticed that the most sensitive parameters are σ_{dm} and σ_{dp} and that they do not strongly depend on the number of events, however, more precise investigation needs to be done. This finding, is an indicator that the proposed LM-HKEM is stable for different datasets having comparable number of events with small tuning for low count. The choice of the parameters here is the result of a preliminary study in terms of CNR and bias with the phantom. The choice of these parameters is important as big values for σ_{dm}, which is related to the MR image, end up with artefacts in the borders between different tissues. From the quality point of view, from Figures 5 and 7 we can appreciate how the kernel method is able to suppress the noise while keeping good resolution and contrast even at extreme situation like low-count.

V. WORK IN PROGRESS

We are currently performing the complete analysis for phantom and patient data. For the short frame cases multiple realizations will be analysed to improve the statistics. The long acquisition reconstructed images will be also analyzed. In addition, the time activity curve (TAC) will be studied for regions like aorta in rabbit data with different reconstruction algorithms, in order to study whether is feasible to improve the image-derived input function (IDIF) from the aorta. Finally, the optimization of the kernel parameters will be more thoroughly studied.
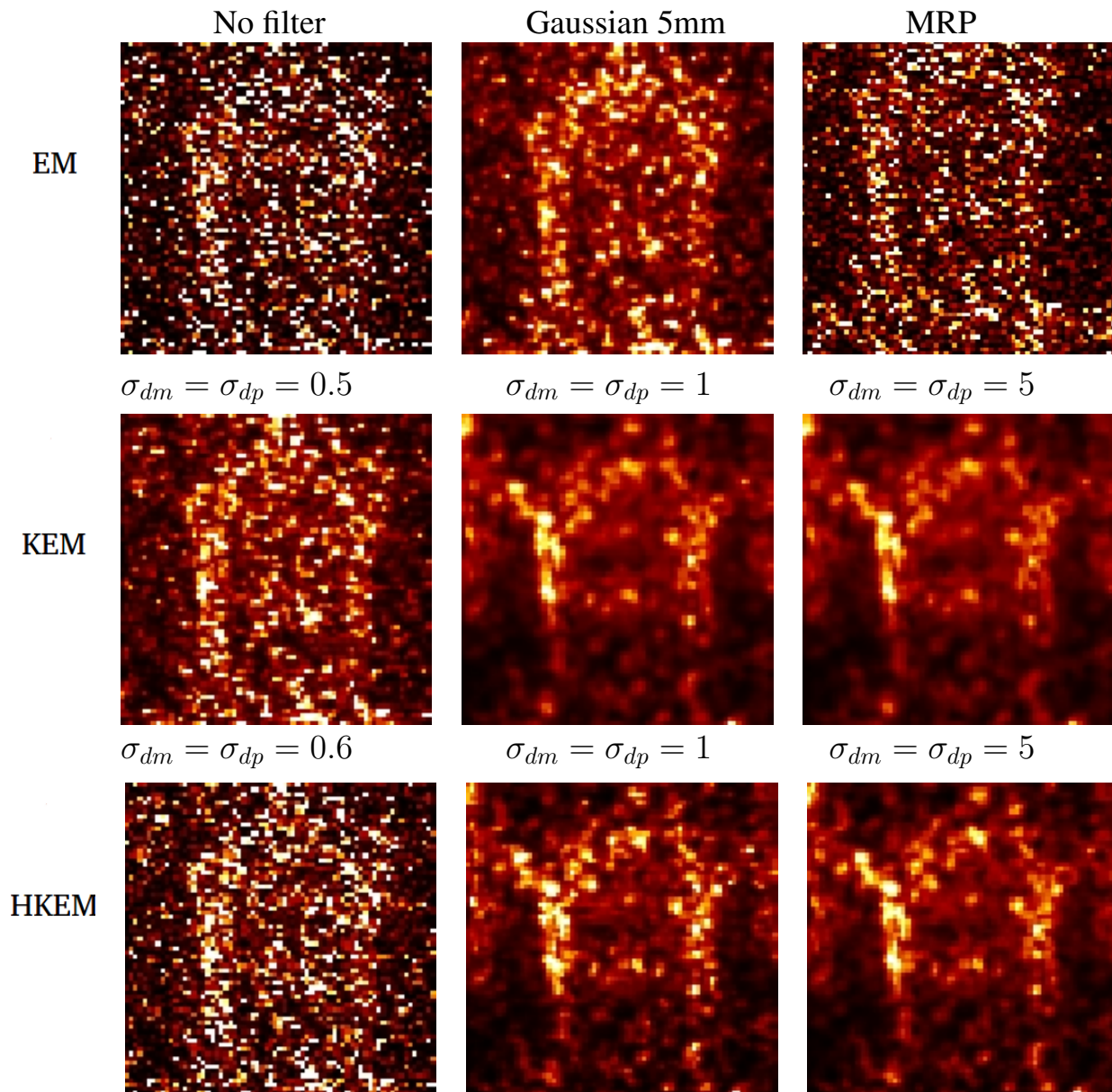
	No filter	Gaussian 5mm	MRP
EM			
KEM	$\sigma_{dm} = \sigma_{dp} = 0.5$	$\sigma_{dm} = \sigma_{dp} = 1$	$\sigma_{dm} = \sigma_{dp} = 5$
HKEM	$\sigma_{dm} = \sigma_{dp} = 0.6$	$\sigma_{dm} = \sigma_{dp} = 1$	$\sigma_{dm} = \sigma_{dp} = 5$

Fig. 7. Reconstructed images with OSEM, OSEM-MRP, KEM using only MR and the proposed method LM-HKEM for a 30 s frame of FDG patient data.

REFERENCES

[1] H. Hudson and R. Larkin, "Accelerated image reconstruction using ordered subsets of projection data," *IEEE Trans. Med. Imaging*, vol. 13, pp. 601–609, 1994.

[2] J. Qi and R. M. Leahy, "Iterative reconstruction techniques in emission computed tomography," *Phys. Med. Biol.*, vol. 51, no. 15, p. R541, 2006.

[3] P. Green, "Bayesian reconstructions from emission tomography data using a modified EM algorithm," *IEEE Trans. Med. Imaging*, vol. 9, pp. 84–93, 1990.

[4] J. Nuyts, D. Beque, P. Dupont, and L. Mortelmans, "A concave prior penalizing relative differences for maximum-a-posteriori reconstruction in emission tomography," *IEEE Trans. Nucl. Sci.*, vol. 49, no. 1, pp. 56–60,
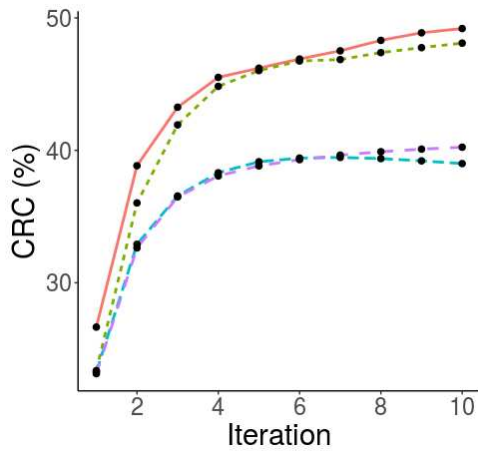
Fig. 6. CRC comparison between reconstructed image with EM, EM-MRP, KEM using only MR and the proposed method HKEM for a 30 s frame of the patient FDG data.
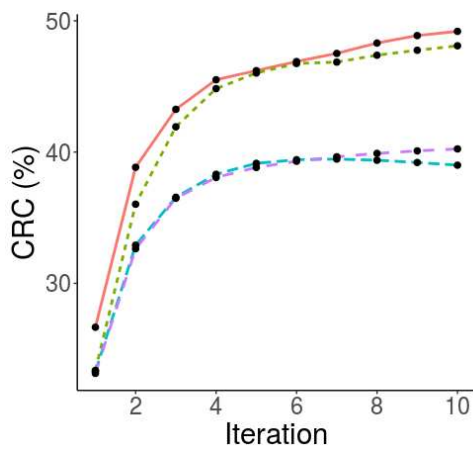

Fig. 8. CRC comparison between reconstructed image with EM, EM-MRP, KEM using only MR and the proposed method HKEM for a 30 s frame of the patient NaF data.

2002.

[5] S. Ahn, S. Ross, E. Asma, J. Miao, X. Jin, L. Cheng, S. Wollenweber, and R. Manjeshwar, "Quantitative comparison of OSEM and penalized likelihood image reconstruction using relative difference penalties for clinical PET," *Phys. Med. Biol.*, vol. 60, pp. 5733–5751, 2015.

[6] R. Leahy and X. Yan, "Incorporation of anatomical MR data for improved functional imaging with PET," in *Inf. Process. Med. Imaging*. Springer, 1991, pp. 105–120.

[7] J. E. Bowsher, V. E. Johnson, T. G. Turkington, R. J. Jaszczak, C. Floyd, and R. E. Coleman, "Bayesian reconstruction and use of anatomical a priori information for emission tomography," *IEEE Trans. Med. Imaging*, vol. 15, no. 5, pp. 673–686, 1996.

[8] J. Tang and A. Rahmim, "Bayesian PET image reconstruction incorporating anato-functional joint entropy," *Phys. Med. Biol.*, vol. 54, no. 23, p. 7063, 2009.

[9] S. Somayajula, C. Panagiotou, A. Rangarajan, Q. Li, S. R. Arridge, and R. M. Leahy, "PET image reconstruc-

tion using information theoretic anatomical priors," *IEEE Trans Med. Imaging*, vol. 30, no. 3, pp. 537–549, 2011.

[10] K. Vunckx, A. Atre, K. Baete, A. Reilhac, C. M. Deroose, K. V. Laere, and J. Nuyts, "Evaluation of three MRI-based anatomical priors for quantitative PET brain imaging," *IEEE Trans. Med. Imaging*, vol. 31, pp. 599–612, 2012.

[11] J. Jiao, N. Burgos, D. Atkinson, B. Hutton, S. Arridge, and S. Ourselin, "Detail-preserving PET reconstruction with sparse image representation and anatomical priors." in *Inf. Proces. Med. Imaging: Proc. Med. Image Comput. Comput. Assist. Interv.*, vol. 24, 2014, pp. 540–551.

[12] F. Knoll, M. Holler, T. Koesters, R. Otazo, K. Bredies, and D. K. Sodickson, "Joint MR-PET reconstruction using a multi-channel image regularizer," *IEEE Trans. Med. Imaging*, vol. 36, no. 1, pp. 1–16, 2017.

[13] L. Parra and H. Barrett, "Maximum-likelihood image reconstruction from list-mode data," *J. Nucl. Med.*, vol. 37, p. 486, 1996.

[14] H. Barrett, T. White, and L. Parra, "List-mode likelihood," *JOSA A*, vol. 14, pp. 2914–2923, 1997.

[15] L. Parra and H. Barrett, "List-mode likelihood: EM algorithm and image quality estimation demonstrated on 2-d PET," *IEEE Trans. Med. Imaging*, vol. 17, pp. 228–235, 1998.

[16] A. J. Reader, S. Ally, F. Bakatselos, R. Manavaki, R. J. Walledge, A. P. Jeavons, P. J. Julyan, S. Zhao, D. L. Hastings, and J. Zweit, "One-pass list-mode EM algorithm for high-resolution 3-D PET image reconstruction into large arrays," *IEEE Trans. Nucl. Sci.*, vol. 49, no. 3, pp. 693–699, 2002.

[17] P. Khurd, I. Hsiao, A. Rangarajan, and G. Gindi, "A globally convergent regularized ordered-subset EM algorithm for list-mode reconstruction," *IEEE Trans. Nucl. Sci.*, vol. 51, pp. 719–725, 2004.

[18] T. Hoffman, B. Scholkopf, and A. Smola, "Kernel methods in machine learning," *Ann. Stat.*, vol. 36, pp. 1171–1220, 2008.

[19] W. Hutchcroft, G. Wang, and J. Qi, "Anatomical-image aided PET reconstruction by the kernel method," *J. Nucl. Med.*, vol. 55, pp. suppl 1, abstract 44, 2014.

[20] W. Hutchcroft, G. Wang, K. T. Chen, C. Catana, and J. Qi, "Anatomically-aided PET reconstruction using the kernel method," *Phys. Med. Biol.*, vol. 61, no. 18, p. 6668, 2016.

[21] G. Wang and J. Qi, "PET image reconstruction using kernel method," *IEEE Trans. Med. Imaging*, vol. 34, pp. 61–71, 2015.

[22] S. Ellis and A. Reader, "Kernelised EM image reconstruction for dual-dataset PET studies," *IEEE MIC, Strasburg, France*, 2016 (in press).

[23] K. Gong, G. Wang, K. Chen, C. Catana, and J. Qi, "Dynamic PET reconstruction using the kernel method with MRI information," *IEEE MIC, Strasburg, France*, 2016 (in press).

[24] P. Novosad and A. Reader, "MR-guided dynamic PET reconstruction with the kernel method and spectral temporal basis functions," *Phys. Med. Biol.*, vol. 61, pp.

4624–4645, 2016.

[25] D. Deidda, N. Efthimiou, R. Manber, K. Thielemans, P. Markiewicz, R. G. Aykroyd, and C. Tsoumpas, "Comparative evaluation of image reconstruction methods for the siemens PET-MR scanner using the STIR library," *IEEE MIC, Strasburg, France*, 2016.

[26] D. Deidda, R. G. Aykroyd, and C. Tsoumpas, "Assessment of maximum a posteriori image estimation algorithms for reduced acquisition time medical positron emission tomography data," *Springer, Contr. to Stat.*, 2017 (in press).

[27] K. Karaoglanis, I. Polycarpou, N. Efthimiou, and C. Tsoumpas, "Appropriately regularized OSEM can improve the reconstructed PET images of data with low count statistics," *Hellenic J. Nucl. Med.*, vol. 18, pp. 140–145, 2015.

[28] M. Walker, M. Asselin, P. Julyan, M. Feldmann, P. Talbot, T. Jones, and J. Matthews, "Bias in iterative reconstruction of low-statistics PET data: benefits of a resolution mode," *Phys. Med. Biol.*, vol. 56, pp. 931–949, 2011.

[29] C. Tsoumpas, P. Aguiar, K. Nikita, D. Ros, and K. Thielemans, "Evaluation of the single scatter simulation algorithm implemented in the STIR library," in *IEEE MIC*, vol. 6, 2004, pp. 3361–3365.

[30] I. Polycarpou, K. Thielemans, R. Manjeshwar, P. Aguiar, P. K. Marsden, and C. Tsoumpas, "Comparative evaluation of scatter correction in 3d PET using different scatter-level approximations," *Annals of Nucl. Med.*, vol. 25, no. 9, pp. 643–649, 2011.

[31] M. W. Jacobson and K. Thielemans, "Optimizability of loglikelihoods for the estimation of detector efficiencies and singles rates in pet," in *IEEE MIC*, 2008, pp. 4580–4586.

[32] D. Hogg, K. Thielemans, T. Spinks, and N. Spyrou, "Maximum-likelihood estimation of normalisation factors for PET," in *IEEE MIC, San Diego, California*, vol. 4, 2001, pp. 2065–2069.

[33] K. Thielemans, C. Tsoumpas, S. Mustafovic, T. Beisel, P. Aguiar, N. Dikaios, and M. Jacobson, "STIR: software for tomographic image reconstruction release 2," *Phys. Med. Biol.*, vol. 57, pp. 867–883, 2012.

[34] M. A. Belzunce and A. J. Reader, "Assessment of the impact of modelling axial compression on PET image reconstruction," *Med. Phys.*, 2017.